Cell Reports

Article

Identification of a second Klotho interaction site in the C terminus of FGF23

Graphical Abstract

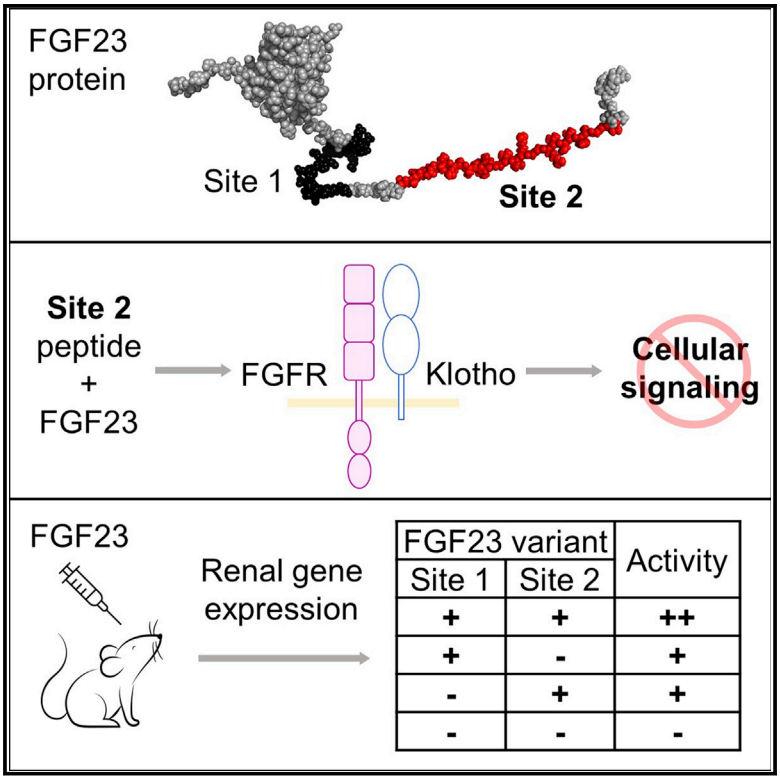

Highlights

- FGF23 C-terminal peptide C28 can interact with KL and function as FGF23 antagonist
- Short peptides of 12 residues can function as competitive FGF23 antagonists
- FGF23 C terminus achieves optimal receptor interaction by 2 functional KL sites
- Selective silencing of either KL site in FGF23 reduces its inherent agonism

Authors

Archita Agrawal, Pu Ni, Rafiou Agoro, Kenneth E. White, Richard D. DiMarchi

Correspondence

rdimarch@indiana.edu

In Brief

Agrawal et al. identify a peptide sequence (C28) in FGF23 that promotes its biological activity and can independently function as an antagonist of Klotho-mediated FGFR activity. FGF23 is a phosphaturic hormone that regulates bone-mineral metabolism and is of medicinal importance for treating bone and kidney disorders.

Agrawal et al., 2021, Cell Reports *34*, 108665
January 26, 2021 © 2021 The Authors.
https://doi.org/10.1016/j.celrep.2020.108665

CellPress

Cell Reports

CellPress
OPEN ACCESS

Article

Identification of a second Klotho interaction site in the C terminus of FGF23

Archita Agrawal,[1] Pu Ni,[2] Rafiou Agoro,[2] Kenneth E. White,[2] and Richard D. DiMarchi[1,3,*]
[1]Department of Chemistry, Indiana University, Bloomington, IN, USA
[2]Department of Medical and Molecular Genetics, Indiana University School of Medicine, Indianapolis, IN, USA
[3]Lead contact
*Correspondence: rdimarch@indiana.edu
https://doi.org/10.1016/j.celrep.2020.108665

SUMMARY

FGF23 interacts with a FGFR/KL-receptor complex to propagate cellular signaling, where its C-terminal C26 peptide is critical for engaging the co-receptor KL. We identify a distinct peptide sequence C28 residing in the FGF23 C terminus that regulates its interaction with KL. C28 can independently function as an FGF23 antagonist, and we report an optimized peptide antagonist of much enhanced potency. FGF23 can use either of the two C-terminal sites to exert biological effects, as shown by *in vitro* and *in vivo* studies. The loss of both KL-interaction sites inactivates the protein. We conclude that the C terminus of FGF23 is a bidentate ligand possessing two independent KL-interaction sites. The identification of this second KL-association site provides an additional perspective in the molecular basis of FGF23-receptor signaling and raises questions pertaining to its structural mechanism of action and the potential for biased biological signaling.

INTRODUCTION

Fibroblast growth factor 23 (FGF23) belongs to the endocrine FGF family of proteins. The *FGF23* gene was discovered as the underlying cause for autosomal dominant hypophosphatemia rickets (ADHR) (White et al., 2000) and tumor-induced osteomalacia (TIO) (Jonsson et al., 2003; Shimada et al., 2001). Genetic mutations at select $Arg^{176,179}$ residues in FGF23 were identified as the molecular basis for hypophosphatemia arising from the sustained action of proteolytically resistant FGF23 proteins (Shimada et al., 2002; White et al., 2001). Subsequently, Shimada et al. (2001, 2004a) and Urakawa et al. (2006) identified that FGF23 regulates phosphate metabolism by its direct action on the kidney. It suppresses the function of the sodium phosphate co-transporter NaPi-2a (SLC34A1) in renal tubules to promote phosphate excretion (Shimada et al., 2004b). Simultaneously, FGF23 reduces circulating 1,25-dihydroxy vitamin D_3 through regulation of the vitamin D-metabolizing enzymes that suppress its synthesis and accelerate catabolism (Saito et al., 2003; Shimada et al., 2004a; Urakawa et al., 2006). These collective actions accelerate phosphate clearance and reduce serum phosphate levels.

At a cellular level, FGF23 activates signaling through a receptor complex of FGF receptor (FGFR) and Klotho (KL) (Kurosu et al., 2006; Urakawa et al., 2006; Yamashita et al., 2002). The N terminus of FGF23 primarily interacts with the FGFR while the C terminus engages KL. The receptor interactions have been elucidated in the crystal structure of the ternary-receptor complex FGF23/FGFR/KL (Chen et al., 2018). The C-terminal truncation of FGF23 up to 48 amino acids did not alter its biological activity (Garringer et al., 2008). Furthermore, competitive FGF23 antagonism with a C-terminally derived FGF23 fragment of 26-amino acid (aa) length (C26, $FGF23^{180–205}$), coupled with structural studies have demonstrated the direct association of this peptide fragment with KL (Chen et al., 2018; Goetz et al., 2010). These results collectively show that a relatively short C-terminal FGF23 peptide supports the receptor interactions leading to downstream biological signaling.

The other endocrine FGFs members (FGF19 and FGF21) use FGFR in the presence of Klotho-β (KLB) to promote their biological action in the liver, adipose, and pancreas. Physiologically FGF19 regulates bile acid metabolism, while FGF21 controls the circulating levels of glucose and lipid (Kuro-o, 2008). The critical interactions between the C terminus of FGF19/FGF21 and their co-receptor KLB have been outlined in their respective crystal structures (Kuzina et al., 2019; Lee et al., 2018). Comparably sized C-terminal peptides of FGF19 and FGF21 can competitively inhibit the activity of these proteins (Agrawal et al., 2018), similar to what is observed with FGF23 C26 and KL (Goetz et al., 2010). These studies promote a biochemical basis of interaction between the endocrine FGFs and their receptor complexes to define a well-aligned C-terminal sequence of ~25 aa that engages with the respective co-receptors KL or KLB. However, it is a mystery why nature extended the C terminus of FGF23 >40 aas beyond the point that has been reported to support its complete biological signaling.

We identified the $FGF23^{212–239}$ sequence (C28) to possess appreciable homology to the reported KL-binding peptide C26 in the extended C terminus of the protein. C28 was determined to be an independent regulator of the interaction of FGF23 with the FGFR/KL complex as first witnessed by the inhibition of FGF23 action. We refined the FGF23 KL-interacting sequence

This is an open access article under the CC BY-NC-ND license (http://creativecommons.org/licenses/by-nc-nd/4.0/).

in peptide 6, which is enhanced by 1 order of magnitude in its ability to block *in vitro* FGF23 activity more than the native C26 or C28. It also antagonizes endogenous FGF23 action in mice. Unexpectedly, we found that unlike the KLB-binding peptides, the KL-peptide antagonists maintain their function when shortened to half the length. The importance of the second KL site for FGF23-protein function is exemplified in the FGF23 A^{188} analog, which preserves bioactivity, despite the functional loss of the first site C26. When both KL-interaction sites are inactivated, the protein is inactive as determined by *in vitro* and *in vivo* studies. This work broadens the current understanding of FGF23-receptor interactions and distinguishes FGF23 from the related FGF19 and FGF21 proteins.

RESULTS

Identification of FGF23 C-terminal peptide C28 interacting with KL and the relationship of structure to activity

Based upon sequence homology, a C-terminal $FGF23^{212–239}$ peptide sequence (C28, also referred to as the second KL site) was identified as a potential KL interaction site (Figures 1A and S1A). Sequence alignment of C28 with the well-characterized KL-binding peptide $FGF23^{180-205}$ (C26, also referred to as first KL-site) displayed 40% identity between the two peptides (Table 1; Figure S1A). The segment (DPLNVLK), which is critical for the interaction of C26 and KL (Chen et al., 2018), was highly conserved in C28 (DPL**G**V**VR**, 3 non-conserved residues in bold font). Four of the 7 amino acids were identical and the last 2 residues were homologous, with only a centrally located glycine as a notable exception (Table 1; Figure S1A). When tested in 293T HEK cells that overexpress the human KL receptor (293/KL), C28 competitively blocked FGF23 signaling at nearly 3-fold enhanced potency relative to C26 (Figure 1B; Table 1). These results indicate that a second FGF23-derived peptide (C28) independent of the reported KL-binding site (C26) is equally capable of antagonizing FGF23 *in vitro* activity. The specificity in KL-dependent signaling was demonstrated by the inability of these FGF23-derived peptides to block FGF21 signaling in 293/KLB cells as compared to the FGF21-associated antagonist ($FGF21^{185–209}$, 21C25) (Figure S1B). The sequence homology in these endocrine FGF peptides ($FGF23^{180–205}$, $FGF23^{212–239}$, $FGF19^{191–216}$, and $FGF21^{185–209}$) is provided in Figure S1A.

We explored the relative basis for activity in the C26 and C28 peptides to determine whether they possess a common structural core for KL binding and whether their inhibitory potency could be enhanced. Reciprocal substitutions within the 2 sequences were made that focused on 3 subsequences with the greatest variation. The first set of peptides sequentially introduced 4 subsequences from C28 to C26 (peptides 1–4), as shown in Table 2. The substitution with the $PMAS^{218–221}$ subsection of C28 in peptide 1 enhanced the antagonistic potency of C26 by 5-fold (Figure 1C; Table 2). The second substitution of $GGRVN^{229–233}$ residues (peptide 2) decreased the potency of C26 by nearly 40-fold, while the third substitution of $HAGGT^{235–239}$ (peptide 3) proved to be of little difference (Figure 1C; Table 2). The last analog of the set consisted of an insertion of 2 amino acids $AS^{220–221}$ (peptide 4), and this produced a 4-fold increase in antagonism (Figure 1C; Table 2). A second set of reciprocal substitutions using subsections of C26 was introduced to C28 (Table 2). The introduction of $ER^{186–187}$ (peptide 5) or $PAPAS^{201–205}$ (peptide 7) resulted in a loss of potency by 4-fold relative to C28 (Figure 1D; Table 2). In contrast, substitution with the pentapeptide $PRARM^{195–199}$ in peptide 6 provided a nearly 10-fold enhancement to the native antagonism of C28 (Figure 1D; Table 2). Peptide 6 proved the most potent of this 28-residue set, and was >20-fold enhanced relative to the previously recognized C26 antagonist (Tables 1 and 2).

We shortened the C26 peptide sequence and surprisingly found retention of significant activity at a length of 14 amino acids (peptide 8, $FGF23^{186–199}$), and even the 12-amino acid peptide (peptide 9, $FGF23^{188–199}$) was a full antagonist of FGF23 but of much reduced potency (Figure 1E; Table 2). An analogous shortening of the most potent chimeric antagonist peptide 6 revealed similar behavior but with enhanced potency relative to C26 at every peptide length studied (peptides 10, 11, and 12; Table 2). The potency of the shortest optimized peptide composed of 12 amino acids (peptide 12) was comparable to C26 (Figure 1F; Tables 1 and 2).

The optimized FGF23 C-terminal peptide is a competitive *in vivo* FGF23 antagonist

C72 and C26 have been reported to modestly modulate serum phosphate levels in normal rodents (Goetz et al., 2010; Johnson et al., 2017). In the parallel KLB-dependent system, FGF19 C-terminal peptides can competitively block FGF19 or FGF21 protein activity at their target organs such as pancreas and adipose tissue (Agrawal et al., 2018). These studies establish a precedent that KL co-receptor-associated *in vivo* bioactivity can be modified by using peptides that function as FGF antagonists *in vitro*.

FGF23 lowers circulating 1,25-dihydroxy vitamin D via the renal activation of vitamin D 24-hydroxylase (*Cyp24a1*) and simultaneous suppression of vitamin D 1α-hydroxylase (*Cyp27b1*) (Saito et al., 2003; Shimada et al., 2004a; Urakawa et al., 2006). To determine whether the FGF23 C-terminal peptide can reverse these effects by blocking endogenous FGF23 action, wild-type (WT) mice were treated with peptide 6 via a single intraperitoneal (i.p.) injection. The kidneys were collected to quantitate gene expression of the vitamin D-regulating enzymes, after 3 or 24 h. The *Cyp24a1* mRNA level was significantly reduced with peptide treatment as compared to saline at 3 h ($p < 0.05$; Figure 2A), and continued to be statistically different at 24 h when compared, respectively, to saline ($p < 0.01$) and peptide treatment ($p < 0.05$). Simultaneously, *Cyp27b1* mRNA was significantly upregulated at 3 h ($p < 0.01$; Figure 2B), and continued to be statistically different at 24 h relative to the saline ($p < 0.05$) and peptide treatment groups ($p < 0.01$). At 24 h, *Cyp27b1* was suppressed relative to saline ($p < 0.05$; Figure 2B).

Site-directed mutagenesis to validate the interaction of the second FGF23 KL site

Structural and biochemical studies have shown that mutation of a single Asp^{188} in the C26 peptide region can inactivate the FGF23 protein (Chen et al., 2018). In an analogous system,

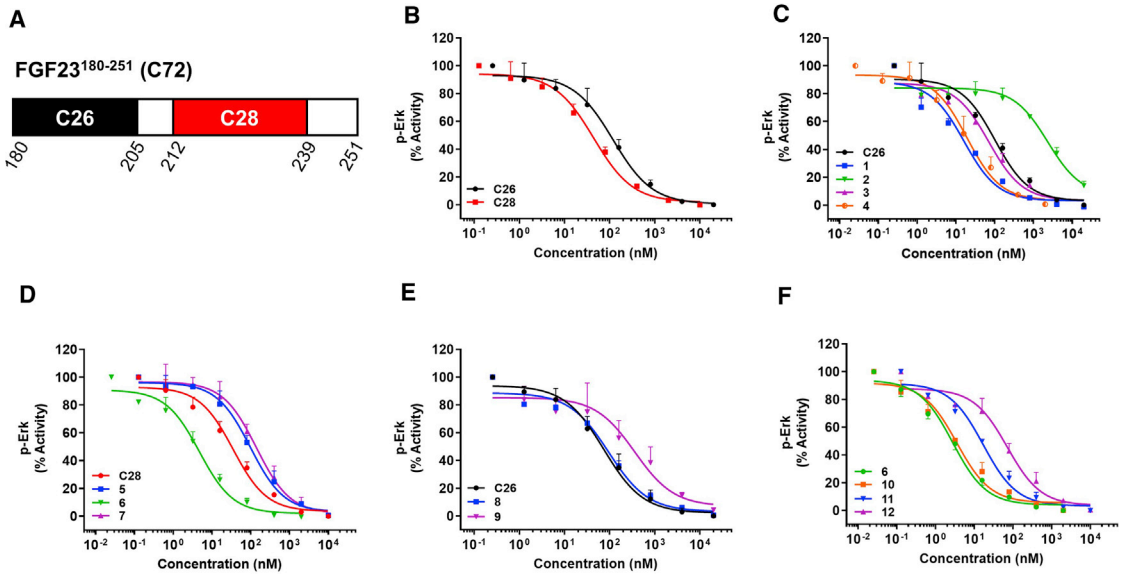

Figure 1. Identification of a second KL-interacting sequence in the C terminus of FGF23, and the structure activity analysis among the 2 KL-interacting peptides C26 and C28

(A) The sequence schematic of the FGF23 C-terminal peptide C72 ($FGF23^{180–251}$), showing the position of the C26 ($FGF23^{180–205}$, black) and the newly identified C28 ($FGF23^{212–239}$, red) peptide.

(B–F) FGF23 antagonism measured by the relative p-Erk levels in 293/KL cells with increasing doses of the peptide antagonist.

(B) C26 (black) or C28 (red).

(C) Effect of the substitutions from C28 sequence into the C26 sequence on the peptide activity, C26 (black), 1 (blue), 2 (green), 3 (pink), and 4 (orange).

(D) Effect of the substitutions from C28 sequence in the C26 sequence on the peptide activity, C28 (red), 5 (blue), 6 (green), and 7 (pink).

(E and F) Determining the shortest effective FGF23 C-terminal peptide antagonist *in vitro* (E) C26 (black), 8 (blue), 9 (pink); (F) 6 (green), 10 (orange), 11 (blue), and 12 (pink). The graphs demonstrate a representative curve for normalized p-Erk response with respect to the response of the standard peptide (B, C, and E) C26, (D) C28, and (F) 6, respectively, means ± SDs, n = 3. Sequence information and potency values presented in Tables 1 and 2.

FGF19 and FGF21 proteins also use the corresponding sequence aligned Asp^{192} to interact with KLB (Agrawal et al., 2018; Kuzina et al., 2019; Lee et al., 2018), and substitution to alanine renders the corresponding C-terminal peptides non-functional as KLB-dependent antagonists. Therefore, we applied an analogous approach to study the interaction between the C termini of FGF23 and KL.

To test whether C28 uses a binding epitope comparable to C26 for interacting with the FGFR/KL complex, we site specifically substituted the central aspartic acid residues (Asp^{188} or Asp^{222}) with an alanine (C26 A1 or C28 A2; Table 1). There was a dramatic loss of antagonistic activity in each peptide resulting from the aspartic acid replacement with alanine (Figure 3A; Table 1). We similarly applied this approach to the fuller-length FGF23 C-terminal peptide of 72-aa length (C72), which harbors both the C26 and C28 peptide sites. The C72 peptide potency proved 70- and 30-fold higher than the individual C26 and C28 peptides, respectively (Table 1). To confirm that the increased potency of C72 was derived from the presence of 2 functional KL sites (C26 and C28) and not the extended peptide length, we studied 2 additional peptides. The peptide with an N-terminal extension of 15 residues to C26 was called C41, and another peptide C40 comprised a C-terminal extension of 12 residues to C28 (Table 1). Each of these peptides revealed a subtly higher potency when compared to the native C26 or C28, respectively (2- to 4-fold; Table 1). However, neither of the extended peptides represents a potency comparable to the native C72 with a half-maximal inhibitory concentration (IC_{50}) of 1.2 nM. Site specific inactivation of each site in C72 by singularly substituting Asp^{188} or Asp^{222} with alanine (C72 A1 or C72 A2) was performed. In each instance, there was a reduction in the inhibitory potency of FGF23 by >20-fold, but each peptide remained of equal to or greater potency than C26 or C28 (Figure 3B; Table 1). When a double substitution of Asp^{188} and Asp^{222} to alanine was made (C72 A1A2), a complete loss of activity was observed (Figure 3B; Table 1).

To further interrogate whether the superior potency of C72 derives from 2 KL-interacting sites or alternatively is a function of increased native sequence size (Figure 3B; Table 1), we engineered a series of dimeric peptide analogs of non-native structure. The peptides C26, C28, or 6 were appended with a pentapeptide C-terminal extension that terminated with a cysteine (Table 2) yielding peptides 13, 14, and 15, respectively. The extension represents a spacer derived from the native FGF23 sequence ($GPEGC^{240–244}$), which follows the C28 sequence. The disulfide homodimers of peptides 13 and 14 were prepared by the direct oxidation of the terminal cysteine to produce peptides 17 and 18 (Table 2). The FGF23-antagonistic potencies of these dimeric peptides were much enhanced (20- to 50-fold) compared to the corresponding monomers and nearly as potent as C72 (Tables 1 and 2). Peptide 19 is the heterodimer formed by 13 and 14, possessing the 2 native

Table 1. *In vitro* antagonistic activities of C-terminal FGF23 peptides

Name	Position	Sequence	IC_{50} ± SD (nM)
C26	$FGF23^{180–205}$	SAEDD SER–DPLNV LKPRA RMTPA PAS	92.3 ± 27.9
C28	$FGF23^{212–239}$	SAED**N** S**PMAS** DPL**G**V **VRGGR VNTH**A **GGT**	36.2 ± 12.1
C26 A1	$FGF23^{180–205}$, A^{188}	–	NC
C28 A2	$FGF23^{212–239}$, A^{222}	–	NC
C72	$FGF23^{180–251}$	SAEDD SER–DPLNV LKPRA RMTPA PAS CSQELP SAED**N** S**PMAS** DPL**G**V **VRGGR VNTH**A **GGT** GPEGC RPFAKFI	1.2 ± 0.5
C41	$FGF23^{165–205}$	PLIHFNTPIPRRHTR SAEDD SER–DPLNV LKPRA RMTPA PAS	27.8 ± 5.6
C40	$FGF23^{212–251}$	SAED**N** S**PMAS** DPL**G**V **VRGGR VNTH**A **GGT** GPEGC RPFAKFI	23.3 ± 7.4
C72 A1	$FGF23^{180–251}$, A^{188}	N/A	24.5 ± 11.5
C72 A2	$FGF23^{180–251}$, A^{222}	N/A	33.1 ± 15.8
C72 A1A2	$FGF23^{180–251}$, $A^{188,222}$	N/A	NC

IC_{50} (half-maximal inhibitory concentration) values (presented in nM, mean ± SD, n = 3) determined by the relative inhibition of FGF23-induced phosphorylation of Erk by increasing concentrations of the peptides tested in 293/KL cells. The peptide sequences are shown with a representative name, native amino acids in 1-letter code, and a short description specifying the position of the peptide in the native FGF23 where applicable. Letters in bold denote the residues of C28 that are not conserved between C26 and C28 peptide sequences, the underlined Asp^{188} and Asp^{222} show the positions of mutagenesis experiments, and the addition of GPEGC sequence in peptides 13–16. IC_{50} values were marked for the analogs that demonstrated negligible activity at the tested concentrations as NC (not calculated).

Table 2. *In vitro* antagonistic activities of C-terminal FGF23 peptides

Name	Position	Sequence	IC_{50} ± SD (nM)
1	–	SAEDD S**PMAS** DPLNV LKPRA RMTPA PAS	18.7 ± 4.7
2	–	SAEDD SER–DPLNV LK**GGR VN**TPA PAS	3,587.0 ± 1,782.7
3	–	SAEDD SER–DPLNV LKPRA RMT**H**A **GGT**	77.7 ± 34.6
4	–	SAEDD SER**AS** DPLNV LKPRA RMTPA PAS	21.3 ± 11.7
5	–	SAED**N** SER–DPL**G**V **VRGGR VNTH**A **GGT**	143.0 ± 77.0
6	–	SAED**N** S**PMAS** DPL**G**V **VR**PRA RMT**H**A **GGT**	3.7 ± 1.2
7	–	SAED**N** S**PMAS** DPL**G**V **VRGGR VN**TPA PAS	157.3 ± 47.9
8	$FGF23^{186–199}$	ER–DPLNV LKPRA RM	97.0 ± 30.3
9	$FGF23^{188–199}$	DPLNV LKPRA RM	542.3 ± 282.0
10	–	**PMAS** DPL**G**V **VR**PRA RM	3.8 ± 0.9
11	–	**AS** DPL**G**V **VR**PRA RM	17.1 ± 0.6
12	–	DPL**G**V **VR**PRA RM	70.9 ± 29.5
13	C26-GPEGC	SAEDD SER–DPLNV LKPRA RMTPA PAS GPEGC	107.3 ± 16.6
14	C28-GPEGC	SAED**N** S**PMAS** DPL**G**V **VRGGR VNTH**A **GGT** GPEGC	57.5 ± 16.3
15	6-GPEGC	SAED**N** S**PMAS** DPL**G**V **VR**PRA RMT**H**A **GGT** GPEGC	5.8 ± 1.1
16	15 A^{222}	SAED**N** S**PMAS** APL**G**V **VR**PRA RMT**H**A **GGT** GPEGC	NC
17	–	13–13 disulfide dimer	2.2 ± 1.2
18	–	14–14 disulfide dimer	3.1 ± 1.8
19	–	13–14 disulfide dimer	2.7 ± 1.3
C26 + C28	–	Non-covalent mixture	15.8 ± 2.2
20	–	15–15 disulfide dimer	1.0 ± 0.4
21	–	16–16 disulfide dimer	NC
22	–	15–16 disulfide dimer	3.4 ± 0.1

The detailed explanation of this table is as provided in the legend to Table 1.

KL-interaction sites of C72, and was indistinguishable from the activity of the 2 homodimers (17 and 18) (Table 2). When the most potent single site FGF23 antagonist (peptide 15) was homodimerized to generate peptide 20, it was of no greater potency than C72, implying that the native C72 represents an upper limit of FGF23 antagonistic potency (Tables 1 and 2). A series of negative controls performed to expectations in which peptides 13, 14, and 15 proved similar to the parent peptides without the pentapeptide extension (Tables 1 and 2). Peptide 16 is identical to 15, except that it possesses the deactivating Asp^{222}Ala substitution and was found to be inactive as expected when tested as a monomer or a dimer (21) (Table 2). In addition, peptide 22, which constitutes a heterodimer of the highly potent peptide 15 and the inactive peptide 16, was reduced in potency relative to C72 and peptide 20 (Tables 1 and 2). These results demonstrate that 2 KL-binding sites increase KL antagonism potency but that there is an upper limit to what is achievable. The magnitude in gain of potency when transitioning from a monomeric to a dimeric entity is prominent in the cases in which dimers are formed from non-optimal monomers (17, 18, and 19), and diminishes when an optimized monomer is dimerized (20).

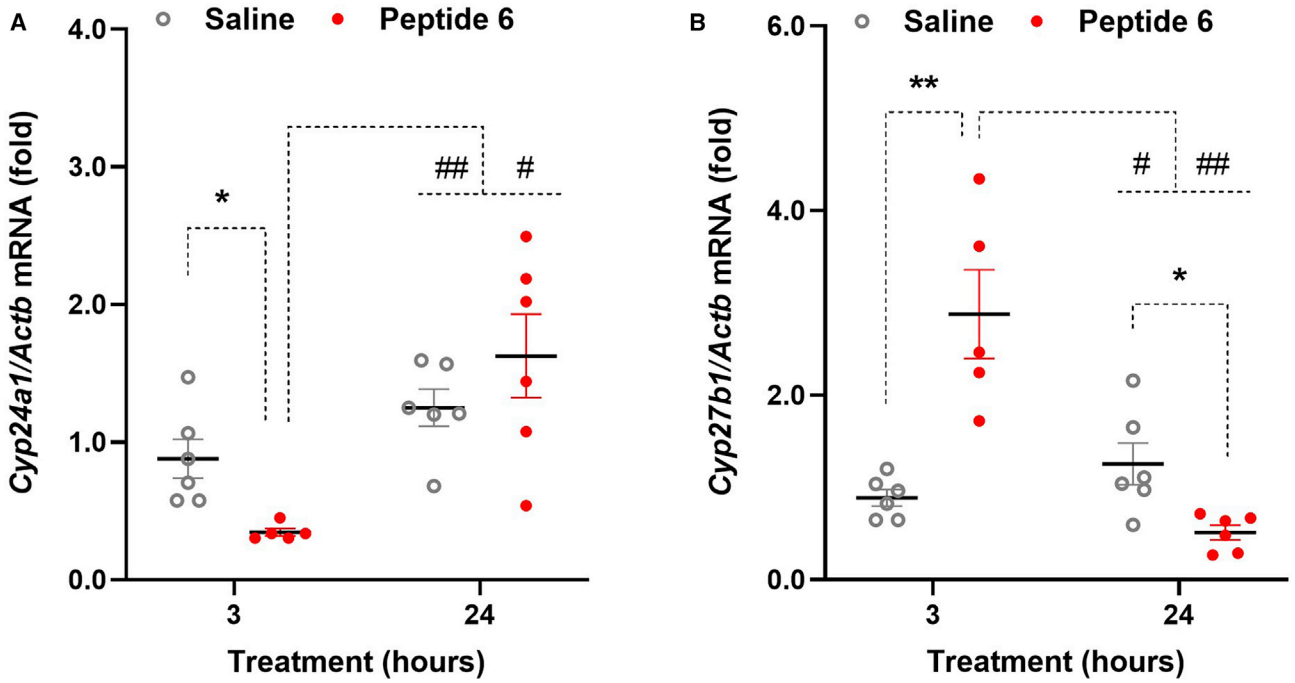

Figure 2. Kidney gene expression modulation by the FGF23-antagonist peptide in mice

WT mice were injected with the FGF23 antagonist peptide 6 (red) at a dose of 30 mg/kg body weight or saline (gray), and kidneys were harvested at 3 or 24 h post-treatment (n = 5 or 6/group). The gene expression markers relevant to FGF23 activity were measured by quantitative real-time PCR (A) *Cyp24a1* and (B) *Cyp27b1*. The data are presented as a scatterplot in which each dot represents 1 animal, mean ± SEM t test with Bonferroni adjustment was used where statistical significance of *p < 0.05 and **p < 0.01 was calculated for peptide treatment versus saline and #p < 0.05 and ##p < 0.01 were calculated for 3-h peptide treatment versus 24-h peptide treatment or 24-h saline, respectively.

Finally, the non-covalent mixing of C26 and C28 demonstrates a slight potency enhancement; however, the magnitude of the change is much smaller than what is observed through a covalent linkage (Table 2).

Demonstration of FGF23 agonism as mediated by the C28 peptide

Whether FGF23-based agonism can use each of the 2 KL-interaction sites as witnessed in the C72 peptide antagonist was studied. To do so, a selective mutation at position Asp^{188} or Asp^{222} was made in the native FGF23. The protein analogs were tested for stimulation of Erk phosphorylation in 293/KL cells, and the A^{222} mutant proved of comparable potency to native protein. This is consistent with prior reports in which C-terminal sequence deletion after residue 205 position had no apparent effect on cellular signaling (Chen et al., 2018; Garringer et al., 2008; Goetz et al., 2010) (Figure 4A; Table S1). To our surprise, we observed that the FGF23, A^{188} analog also retained full potency with no discernible difference relative to native FGF23. Asp^{188} residue is purported to be singularly essential for KL binding and FGF23 activity (Chen et al., 2018), and its importance was substantiated by the lack of antagonism when the C26 peptide was similarly mutated from Asp to Ala (Figure 3A). This result suggests that in the absence of a functional C26 KL site, the downstream C28 KL site enables FGF23 to productively signal through the FGFR/KL complex. When the Asp^{188} and Asp^{222} residues of FGF23 were both mutated to alanine ($A^{188,222}$ analog), the bioactivity was abrogated (Figure 4A; Table S1). To confirm that these observations did not result from unexpected changes in higher-order structure that was not apparent in biosynthesis, purification, or formulation of the mutant proteins, we directly assessed their biophysical integrity by thermal denaturation (Figure S2).

To further explore the function of the second KL site, we investigated the prospect that possessing 2 sites may prove advantageous in a specific context in which the FGFR binding element is less than optimal. The N-terminal domain of the endocrine FGFs primarily determines the FGFR activation while the C-terminal sequence guides the co-receptor specificity with a Klotho co-receptor, KL or KLB (Micanovic et al., 2009; Yie et al., 2009, 2012). The receptor complex specificity among the endocrine FGF proteins can be modulated by altering their C-terminal domains (Wu et al., 2008, 2012). Consequently, we prepared 2 FGF21–23 chimeric protein analogs containing the FGF21 N-terminal core, with its C-terminal KLB-binding peptide replaced with an FGF23 C-terminal peptide sequence constituted by C72 (FGF21–23 C72) or C26 (FGF21–23 C26) (Table S1). Native FGF21 was unable to activate the FGFR/KL complex as expected, but the FGF21–23 C72 analog demonstrated a sub-nanomolar FGFR activation (half-maximal effective concentration [EC_{50}] 0.2 nM) and partial agonism as compared to native FGF23 (Figure S3; Table S1). The single KL site FGF21 analog (FGF21–23 C26, EC_{50} 197.3 nM) was 1,000-fold less potent than the double KL site FGF21–23 C72 analog (Figure S3; Table

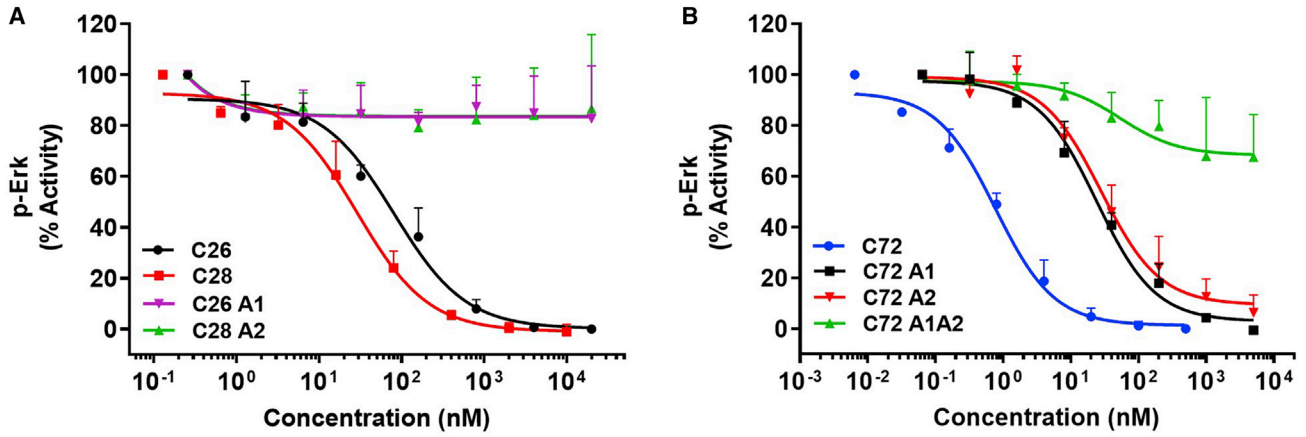

Figure 3. Mutation of the C-terminal FGF23 peptides to assess their KL-interaction site by study of FGF23-activity antagonism in 293/KL cells

(A and B) FGF23 C-terminal peptides tested for their ability to block FGF23-signaling measured by relative p-Erk levels (A) C26 (black), C28 (red), C26 A1 (pink, $FGF23^{180–205}$, A^{188}), and C28 A2 (green, $FGF23^{212–239}$, A^{222}) and (B) C72 (blue, $FGF23^{180–251}$), C72 A1 (black, $FGF23^{180–251}$, A^{188}), C72 A2 (red, $FGF23^{180–251}$, A^{222}), and C72 A1A2 (green, $FGF23^{180–251}$, $A^{188,222}$). The graphs demonstrate a representative curve for normalized p-Erk response with respect to the response of the standard peptide (A) C26 and (B) C72, respectively; means ± SDs, n = 3. Sequence information and potency values presented in Table 1.

S1). These results confirm our hypothesis that while the individual KL site mutations in FGF23 did not diminish *in vitro* efficacy, the absence of the second site in an unoptimized FGFR ligand dramatically decreases agonism.

To test whether C28 as the second KL-interaction site can promote FGF23 *in vivo* activity, the single-site FGF23 analogs were assessed for their ability to alter kidney gene expression in normal mice. Four proteins (FGF23, FGF23 A^{188}, FGF23 A^{222}, or FGF23 $A^{188,222}$ analogs) were each dosed in mice 0.5 mg/kg, and 3 h later, quantitative real-time PCR was used to assess kidney mRNA expression of the FGFR/KL-downstream targets *Cyp24a1*, *Cyp27b1*, and early growth response protein 1 *(Egr1)*. A significant elevation of *Cyp24a1* along with coordinate suppression of *Cyp27b1* was recorded for FGF23, FGF23 A^{188}, and FGF23 A^{222} as compared to vehicle treatment ($p < 0.001$; Figures 4B and 4C). For *Egr1*, FGF23 showed a statistically significant change as compared to vehicle ($p < 0.001$), while single-site mutants showed only a trend to activation (Figure 4D). This is not surprising since the optimal treatment time for *Egr1* modulation is as early as 1 h for FGF-signaling measurements (Agrawal et al., 2018; Portale et al., 2015).

The magnitude in the upregulation of gene expression for *Cyp24a1* was the highest, with 20-fold induction by native FGF23 treatment (Figure 4B). For this particular target, we clearly see that at the single administered dose of FGF23 A^{188} or FGF23 A^{222}, the magnitude of the effect was fractionally reduced as compared to native FGF23 ($p < 0.01$; Figure 4B). Similarly, we observe the *Egr1* induction to be reduced for FGF23 A^{188} and FGF23 A^{222} analogs as compared to native FGF23 ($p < 0.05$; Figure 4D), but no difference is observed among the analogs and FGF23 for *Cyp27b1* (Figure 4C).

Of importance, the doubly mutated FGF23 $A^{188,222}$ proved inactive relative to the native protein and the single-site mutants ($p < 0.001$ for *Cyp24a1* and *Cyp27b1*; Figures 4B and 4C), and similar to the vehicle-treated group. For *Egr1*, the FGF23 $A^{188,222}$ was statistically different as compared to FGF23 treatment ($p < 0.01$; Figure 4D), and reduced when compared to the single-site mutants but determined not to be statistically significant. Collectively, these results corroborate the existence of 2 distinct KL sites to support FGF23 bioactivity at molecular targets of physiological relevance. Furthermore, the differential *Cyp24a1* activity (Figure 4B) indicates that complete efficacy in biological signaling is only achieved when both KL sites are functional.

DISCUSSION

The identification of FGF23 as a phosphaturic hormone was a major advance in the physiology of phosphate metabolism. The finding of the FGF23 gene mutations in ADHR patients (White et al., 2000) was subsequently extended to other diseases, including TIO (Shimada et al., 2001), X-linked hypophosphatemia (XLH) (Jonsson et al., 2003), and familial tumor calcinosis (Econs, 2017; Sitara et al., 2004). Given its role in the regulation of bone-mineral metabolism, the FGF23 pathway has emerged as a therapeutic target to address a range of bone-mineral and kidney disorders (Fukumoto, 2016). The neutralizing FGF23 antibody burosumab has reported efficacy in the treatment of hypophosphatemia and is registered for the treatment of XLH (Collins, 2018). The therapeutic use of the C-terminal peptide C72 has also been proposed for the treatment of hypophosphatemia (Goetz et al., 2010; Johnson et al., 2017) and renal anemia (Agoro et al., 2018). The potential for the broadened use of FGF antagonism in the treatment of chronic kidney disease remains exploratory as a study in rats reported improved overall disease symptoms, but it exacerbated mineral imbalance and was associated with higher mortality (Shalhoub et al., 2012).

The C26 peptide is a competitive FGF23 antagonist (Goetz et al., 2010), and its direct interaction with KL is supported by the structural data (Chen et al., 2018). This KL-binding site is critical for FGFR/KL-receptor activation, and deletion of the

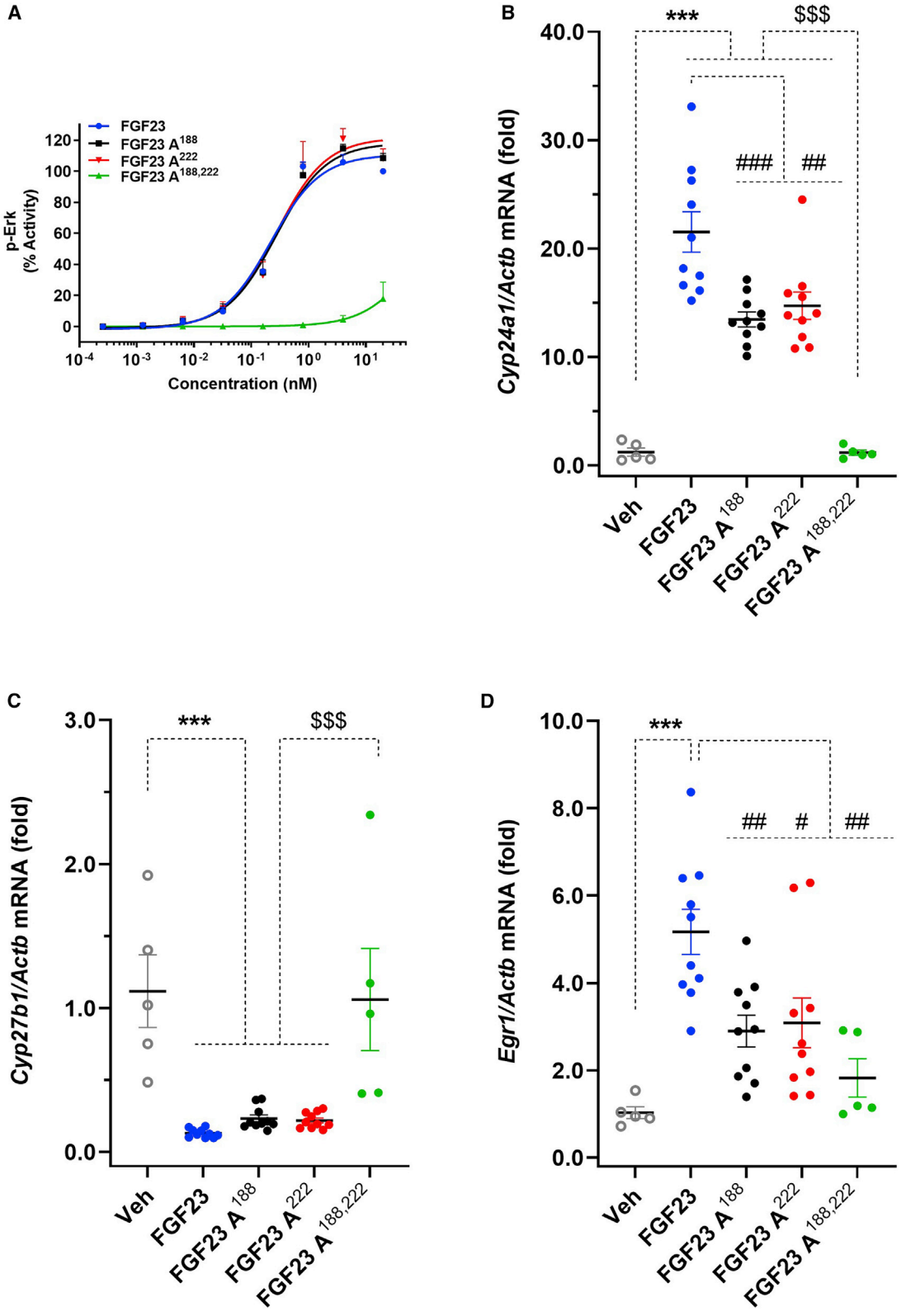

(legend on next page)

remainder of the FGF23 C terminus is of no reported consequence to cellular activity (Chen et al., 2018; Garringer et al., 2008; Goetz et al., 2010). This envisioned molecular mechanism of action in FGF23 signaling aligns with that of the related endocrine FGF proteins FGF19 and FGF21. All 3 FGFs use homologous linear C-terminal sequences of ~25 aas to bind a specific KL co-receptor. In each instance, the peptide as an independent fragment can competitively and selectively antagonize native protein signaling (Agrawal et al., 2018; Kuzina et al., 2019; Lee et al., 2018). Unlike FGF19 and FGF21, in which the protein sequence terminates with the KLB-binding site, FGF23 is extended by an additional 46 aas, representing a 20% increase in the full protein size. This raises the question of whether this extended sequence is of any importance to the biological function of the hormone, specifically as it relates to the FGF23-receptor complex interaction.

Within the extended portion of the FGF23 C-terminal previously suspected to have no biological function, we identified a sequence (C28) of partial homology to the known KL-binding site (C26) that can similarly function as a competitive peptide-based FGF23 antagonist (Figures 1A and 1B; Table 1). Structural modeling of C28 peptide using the reported structure of C26 peptide (Chen et al., 2018) as a template suggests that the sequence-aligned $C28^{222–227}$ residues that are central to facilitating C26/KL interaction can adopt a similar structure and, as such, appear capable of using a similar mechanism to interact with KL (Figures S1A and S4). However, it must be noted that C26 and C28 share limited sequence identity (40%), and it remains possible that they each possess different interactions with KL. We have shown by detailed structure activity analysis that the $PRARM^{195–199}$ sequence in C26 and the $PMAS^{218–221}$ sequence in C28 can be integrated into a chimeric peptide that demonstrates higher potency FGF23 antagonism than either of the native KL-interaction sites (Figures 1C and 1D; Table 2). The structurally optimized antagonist that we identified (peptide 6) is of 20-fold higher potency (IC_{50} 3.7 nM) than the known KL-binding site (C26) and 10-fold enhanced relative to the second site (C28). In each of the peptides C26 and C28, the site-specific mutation of an aspartic acid of known importance to KL binding destroyed the bioactivity of the peptide (Figure 3A; Table 1). Extending these studies to the C72 peptide revealed a 20-fold potency reduction when either of the 2 sites was individually inactivated (Figure 3B; Table 1), but the peptides retained the activity corresponding to the shorter C26 and C28 peptides. A previous study that measured the binding affinities of C26 and C72 peptides with the FGFR/KL complex, revealed that the longer C72 peptide had a higher affinity for interaction with the receptor as compared to the shorter C26 peptide (Goetz et al., 2010). Our results align with this observation: we propose that C72 possesses 2 individual KL-binding peptides resulting in a higher potency for association with the receptor complex, as compared to that of individual peptides. Of note, when both sites are inactivated, the FGF23 antagonism by C72 is lost (Figure 3B; Table 1). These results collectively confirm the presence of a second functional sequence residing in the C terminus of FGF23 that can regulate interactions in the FGFR complex and significantly enhance the potency of KL interaction in concert with the first site.

The length of the smallest functional KL-peptide antagonist was unexpectedly much shorter than what was anticipated based upon similar truncation in KLB-binding peptides and their ability to inhibit FGF19 or FGF21 agonism (Agrawal et al., 2018). A reduction of just 2 amino acids in these peptide antagonists of ~25 amino acids resulted in the severe loss of KLB-dependent inhibition (Agrawal et al., 2018). A shortening to only 12 aas in the sequence-optimized antagonist yielded peptide 12, with a potency that is equivalent to that of the native C26 peptide (Figure 1F; Table 2). This observation indicates that there are striking differences in the requirements for high-potency interactions at the 2 structurally related KL co-receptors (KL and KLB), and suggests that the structural basis for FGF agonism may not be as conserved as previously envisioned. Furthermore, in a pragmatic sense, the reduction of the KL-mediated FGF23 inhibition to as little as a 12-aa peptide represents a sizable advancement in therapeutic antagonists for treating bone-mineral diseases, in which burosumab is 100 times larger in molecular size and represents a highly expensive medicine. The optimized antagonist peptide 6, when administered to mice, altered the renal gene expression of the vitamin D-metabolizing enzymes *Cyp24a1* and *Cyp27b1* (Figure 2), indicative of the successful suppression of endogenous FGF23-mediated physiological targets.

Based upon the observation that C72 demonstrates higher activity than the individual peptides, dimeric forms of C26 and C28 were prepared (peptides 17, 18, and 19). These peptides were ~20- to 50-fold more potent than their respective monomers, achieving a potency that is competitive with C72 (Table 2). We propose that having 2 KL-interaction sequences (covalently linked as a single entity) provides a thermodynamic advantage for a more efficient KL association. In analogous fashion, a fully functional antibody achieves its composite antagonist potency by the sum of the strength constituted by 2 individual antibody binding sites with a common antigen. The dimer of the optimized peptide 6, peptide 20, is only slightly enhanced relative to the other peptide dimers to achieve a potency equal to that of C72 (Table 2). As the potency of the monomeric peptides increases,

Figure 4. Determining the activities of FGF23 analogs containing 1 or 2 active KL-interaction sites by *in vitro* and *in vivo* methods

(A) *In vitro* assessment of FGF23-signaling activity as measured by relative p-Erk levels in 293/KL cells, FGF23 (blue), FGF23 A^{188} (black), FGF23 A^{222} (red), and FGF23 $A^{188,222}$ (green); the graph demonstrates a representative curve for normalized p-Erk response with reference to the standard FGF23 response; means ± SDs, n = 3. The potency values are presented in Table S1.

(B–D) *In vivo* assessment of FGF23 activity in mice. WT mice were treated with 0.5 mg/kg body weight with either FGF23 (blue), FGF23 A^{188} (black), FGF23 A^{222} (red), FGF23 $A^{188,222}$ (green), or vehicle (gray); n = 5 or 10/group, and post-3 h the gene expression changes were studied by quantitative real-time PCR for target genes, (B) *Cyp24a1*, (C) *Cyp27b1*, and (D) *Egr1*. The data are presented as a scatterplot in which each dot represents 1 animal; mean ± SEM. One-way ANOVA with Tukey's comparison was used for statistical analyses in which ***p < 0.001 versus vehicle, #p < 0.05, ##p < 0.01, ###p < 0.001 versus FGF23, and $$$p < 0.001 versus FGF23 $A^{188,222}$ were calculated.

the relative gain through dimerization is limited to the apparent upper limit of interaction with KL (Table 2).

Having established the presence of a second KL-association site in the C terminus of FGF23 and the enhanced antagonistic potency with 2 functional sites, we investigated whether FGF23 agonism is similarly supported by 2 sites. The individual mutation of Asp^{188} or Asp^{222} did not change FGF23 activity in 293/KL cells, while the double mutation destroyed FGF23 activity (Figure 4A; Table S1). The results establish that each of the 2 sites is equally and independently capable of supporting FGF23 agonism, but unlike the study of antagonism in the C72 C-terminal peptide (Figure 3B), there was no apparent additivity in the double-site functioning protein relative to the single-site mutants. We hypothesized that this could result from the highly optimized nature of the native FGF23 when studied in the engineered 293/KL cells that overexpress the KL co-receptor to achieve enhanced signal to noise, making it less amenable to observe finer downstream signaling changes. We explored this prospect through the synthesis of a less optimal FGF23 mimetic in which the N-terminal domain was provided by FGF21 and paired with 1 of 2 FGF23 C-terminal sequence extensions. A significant difference in the bioactivity was recorded for a FGF21–23 C72 chimeric protein that contains both KL-interaction sequences relative to a comparable but shorter chimeric protein FGF21–23 C26, which contains only a single KL-interaction site (Figure S3; Table S1). These results are supportive of the hypothesis that the benefit of having 2 sites relative to 1 is most evident *in vitro*, when less-than-optimal interactions comprise the ternary-receptor complex.

To study the contribution of each KL-interaction site to native FGF23 function in a physiological setting, we administered the FGF23 analogs to normal mice and examined the kidney as a representative target tissue. Native FGF23 provides a statistically significant change in the gene expression for the vitamin D-metabolizing enzymes *Cyp24a1* and *Cyp27b1*, as well as *Egr1* (Figures 4B–4D) ($p < 0.001$), compared to vehicle treatment for each of the targets. The doubly mutated FGF23 $A^{188,222}$ analog with inactivating mutations in both KL sites was devoid of *in vivo* activity, which is consistent with the absence of *in vitro* activity (Figure 4). The FGF23 A^{188} or FGF23 A^{222} analogs in which 1 of the 2 KL sites is individually inactivated, demonstrated kidney target gene regulation directionally consistent with native FGF23 in a statistically significant manner ($p \leq 0.001$) as compared to vehicle treatment for *Cyp24a1* and *Cyp27b1* (Figure 4B and 4C). This supports the conclusion that the C28 sequence is of functional importance for KL interaction, and the protein retains its activity in the absence of 1 of the 2 functioning KL sites. Of note, the FGF3 A^{188} or FGF23 A^{222} analogs were less efficacious at inducing gene expression as compared to native FGF23 at a single equivalent dose of 0.5 mg/kg, most clearly seen in the instance of *Cyp24a1* (Figure 4B; $p < 0.01$). Coupled with the absence of bioactivity of the double mutant, it can be concluded that both sites are required to achieve full *in vivo* bioactivity. It is also possible that the pharmacokinetics of the native hormone are enhanced in total exposure or duration, despite comparable physical properties and the subtle nature of the structural change to the protein. Dose titration and direct pharmacokinetic measures are required to determine whether there are differences in the specific *in vivo* potency of the single KL-site protein mutants. Nonetheless, the dovetailed *in vitro* and *in vivo* results presented here with peptide antagonists and protein agonists clearly establish the presence of a second KL site in the C-terminal fragment of FGF23, which was previously unrecognized.

In summary, we present evidence of a second KL site (C28) in native FGF23 capable of biological function and necessary for full FGF23 activity. The occurrence of C26 and C28 peptides in the FGF23 C terminus appears different relative to FGF19 and FGF21, in which signaling through the KLB co-receptor occurs through a single KLB-binding site. How this second site may be structurally coordinated to engage the FGFR/KL complex remains to be defined. The prospect that these 2 sites may yet prove to have overlapping but differing biological function, so-called biased agonism, remains to be determined. In addition, we report a highly potent peptide antagonist suitable for therapeutic use, and demonstrate that the minimal binding epitope for KL antagonists is as small as 12 aas. The observations presented in this article should encourage continued investigation of the molecular mechanism of FGF23 signaling and the associated physiological consequences, while further defining the basis of evolution within the 3 distinct endocrine FGF hormones.

STAR★METHODS

Detailed methods are provided in the online version of this paper and include the following:

- KEY RESOURCES TABLE
- RESOURCE AVAILABILITY
  - Lead contact
  - Materials availability
  - Data and code availability
- EXPERIMENTAL MODEL AND SUBJECT DETAILS
  - Animals
  - Cell lines
- METHOD DETAILS
  - Peptide synthesis
  - Protein synthesis
  - Purity and concentration estimation of the peptides and proteins
  - pERK AlphaLISA assay
  - Protein Thermal Shift
  - *In vivo* studies
  - Quantitative real time PCR
  - Structural modeling of C28 peptide
- QUANTIFICATION AND STATISTICAL ANALYSIS
  - Cellular signaling data analysis
  - Gene expression data analysis of *in vivo* studies

SUPPLEMENTAL INFORMATION

Supplemental Information can be found online at https://doi.org/10.1016/j.celrep.2020.108665.

ACKNOWLEDGMENTS

We thank Drs. Pengyun Li and Alexei Kharitonenkov for the assembly of the 293THEK/hKL- and hKLB-expressing cell lines. We thank Drs. Piotr Mroz and Fa Zhang for assistance with the peptide synthesis. We thank Dr. Giovanni Gonzalez-Gutierrez for assistance with modeling the C28 peptide. Research funding was provided by the Gill Research Center at Indiana University.

AUTHOR CONTRIBUTIONS

A.A. designed, performed, and analyzed the peptide and protein synthesis and the *in vitro* experiments. P.N. designed, performed, and analyzed the *in vivo* studies. A.A., P.N., R.A., K.E.W., and R.D.D. collectively designed studies and interpreted the data. A.A. and R.D.D. wrote the manuscript.

DECLARATION OF INTERESTS

K.E.W. receives royalties from Kyowa-Hakko-Kirin Pharmaceutics, Inc. for licensing the FGF23 gene through Indiana University. A patent application pertaining to peptide antagonists of FGF23 has been filed by Indiana University. The authors and our immediate families have no other financial interests to declare, have no positions to declare, and are not members of the journal's advisory board.

Received: August 31, 2020
Revised: November 13, 2020
Accepted: December 24, 2020
Published: January 26, 2021

REFERENCES

Agoro, R., Montagna, A., Goetz, R., Aligbe, O., Singh, G., Coe, L.M., Mohammadi, M., Rivella, S., and Sitara, D. (2018). Inhibition of fibroblast growth factor 23 (FGF23) signaling rescues renal anemia. FASEB J. *32*, 3752–3764.

Agrawal, A., Parlee, S., Perez-Tilve, D., Li, P., Pan, J., Mroz, P.A.P.A., Kruse Hansen, A.M.A.M., Andersen, B., Finan, B., Kharitonenkov, A., and DiMarchi, R.D. (2018). Molecular elements in FGF19 and FGF21 defining KLB/FGFR activity and specificity. Mol. Metab. *13*, 45–55.

Chen, G., Liu, Y., Goetz, R., Fu, L., Jayaraman, S., Hu, M.C., Moe, O.W., Liang, G., Li, X., and Mohammadi, M. (2018). α-Klotho is a non-enzymatic molecular scaffold for FGF23 hormone signalling. Nature *553*, 461–466.

Collins, M. (2018). Burosumab: At Long Last, an Effective Treatment for FGF23-Associated Hypophosphatemia. J. Bone Miner. Res. *33*, 1381–1382.

Econs, M.J. (2017). Genetic diseases resulting from disordered FGF23/klotho biology. Bone *100*, 56–61.

Fukumoto, S. (2016). FGF23-FGF Receptor/Klotho Pathway as a New Drug Target for Disorders of Bone and Mineral Metabolism. Calcif. Tissue Int. *98*, 334–340.

Garringer, H.J., Malekpour, M., Esteghamat, F., Mortazavi, S.M.J., Davis, S.I., Farrow, E.G., Yu, X., Arking, D.E., Dietz, H.C., and White, K.E. (2008). Molecular genetic and biochemical analyses of FGF23 mutations in familial tumoral calcinosis. Am. J. Physiol. Endocrinol. Metab. *295*, E929–E937.

Goetz, R., Nakada, Y., Hu, M.C., Kurosu, H., Wang, L., Nakatani, T., Shi, M., Eliseenkova, A.V., Razzaque, M.S., Moe, O.W., et al. (2010). Isolated C-terminal tail of FGF23 alleviates hypophosphatemia by inhibiting FGF23-FGFR-Klotho complex formation. Proc. Natl. Acad. Sci. USA *107*, 407–412.

Johnson, K., Levine, K., Sergi, J., Chamoun, J., Roach, R., Vekich, J., Favis, M., Horn, M., Cao, X., Miller, B., et al. (2017). Therapeutic Effects of FGF23 c-tail Fc in a Murine Preclinical Model of X-Linked Hypophosphatemia Via the Selective Modulation of Phosphate Reabsorption. J. Bone Miner. Res. *32*, 2062–2073.

Jonsson, K.B., Zahradnik, R., Larsson, T., White, K.E., Sugimoto, T., Imanishi, Y., Yamamoto, T., Hampson, G., Koshiyama, H., Ljunggren, O., et al. (2003). Fibroblast growth factor 23 in oncogenic osteomalacia and X-linked hypophosphatemia. N. Engl. J. Med. *348*, 1656–1663.

Kuro-o, M. (2008). Endocrine FGFs and Klothos: emerging concepts. Trends Endocrinol. Metab. *19*, 239–245.

Kurosu, H., Ogawa, Y., Miyoshi, M., Yamamoto, M., Nandi, A., Rosenblatt, K.P., Baum, M.G., Schiavi, S., Hu, M.C., Moe, O.W., and Kuro-o, M. (2006). Regulation of fibroblast growth factor-23 signaling by klotho. J. Biol. Chem. *281*, 6120–6123.

Kuzina, E.S., Ung, P.M.U., Mohanty, J., Tome, F., Choi, J., Pardon, E., Steyaert, J., Lax, I., Schlessinger, A., Schlessinger, J., and Lee, S. (2019). Structures of ligand-occupied β-Klotho complexes reveal a molecular mechanism underlying endocrine FGF specificity and activity. Proc. Natl. Acad. Sci. USA *116*, 7819–7824.

Lee, S., Choi, J., Mohanty, J., Sousa, L.P., Tome, F., Pardon, E., Steyaert, J., Lemmon, M.A., Lax, I., and Schlessinger, J. (2018). Structures of β-klotho reveal a 'zip code'-like mechanism for endocrine FGF signalling. Nature *553*, 501–505.

Livak, K.J., and Schmittgen, T.D. (2001). Analysis of relative gene expression data using real-time quantitative PCR and the 2(-Δ Δ C(T)) Method. Methods *25*, 402–408.

Micanovic, R., Raches, D.W., Dunbar, J.D., Driver, D.A., Bina, H.A., Dickinson, C.D., and Kharitonenkov, A. (2009). Different roles of N- and C- termini in the functional activity of FGF21. J. Cell. Physiol. *219*, 227–234.

Portale, A.A., Zhang, M.Y.H., David, V., Martin, A., Jiao, Y., Gu, W., and Perwad, F. (2015). Characterization of FGF23-dependent Egr-1 cistrome in the mouse renal proximal tubule. PLoS ONE *10*, e0142924.

Saito, H., Kusano, K., Kinosaki, M., Ito, H., Hirata, M., Segawa, H., Miyamoto, K., and Fukushima, N. (2003). Human fibroblast growth factor-23 mutants suppress Na+-dependent phosphate co-transport activity and 1α,25-dihydroxyvitamin D3 production. J. Biol. Chem. *278*, 2206–2211.

Shalhoub, V., Shatzen, E.M., Ward, S.C., Davis, J., Stevens, J., Bi, V., Renshaw, L., Hawkins, N., Wang, W., Chen, C., et al. (2012). FGF23 neutralization improves chronic kidney disease-associated hyperparathyroidism yet increases mortality. J. Clin. Invest. *122*, 2543–2553.

Shimada, T., Mizutani, S., Muto, T., Yoneya, T., Hino, R., Takeda, S., Takeuchi, Y., Fujita, T., Fukumoto, S., and Yamashita, T. (2001). Cloning and characterization of FGF23 as a causative factor of tumor-induced osteomalacia. Proc. Natl. Acad. Sci. USA *98*, 6500–6505.

Shimada, T., Muto, T., Urakawa, I., Yoneya, T., Yamazaki, Y., Okawa, K., Takeuchi, Y., Fujita, T., Fukumoto, S., and Yamashita, T. (2002). Mutant FGF-23 responsible for autosomal dominant hypophosphatemic rickets is resistant to proteolytic cleavage and causes hypophosphatemia in vivo. Endocrinology *143*, 3179–3182.

Shimada, T., Hasegawa, H., Yamazaki, Y., Muto, T., Hino, R., Takeuchi, Y., Fujita, T., Nakahara, K., Fukumoto, S., and Yamashita, T. (2004a). FGF-23 is a potent regulator of vitamin D metabolism and phosphate homeostasis. J. Bone Miner. Res. *19*, 429–435.

Shimada, T., Kakitani, M., Yamazaki, Y., Hasegawa, H., Takeuchi, Y., Fujita, T., Fukumoto, S., Tomizuka, K., and Yamashita, T. (2004b). Targeted ablation of Fgf23 demonstrates an essential physiological role of FGF23 in phosphate and vitamin D metabolism. J. Clin. Invest. *113*, 561–568.

Sitara, D., Razzaque, M.S., Hesse, M., Yoganathan, S., Taguchi, T., Erben, R.G., Jüppner, H., and Lanske, B. (2004). Homozygous ablation of fibroblast growth factor-23 results in hyperphosphatemia and impaired skeletogenesis, and reverses hypophosphatemia in Phex-deficient mice. Matrix Biol. *23*, 421–432.

Urakawa, I., Yamazaki, Y., Shimada, T., Iijima, K., Hasegawa, H., Okawa, K., Fujita, T., Fukumoto, S., and Yamashita, T. (2006). Klotho converts canonical FGF receptor into a specific receptor for FGF23. Nature *444*, 770–774.

White, K.E., Evans, W.E., O'Riordan, J.L.H., Speer, M.C., Econs, M.J., Lorenz-Depiereux, B., Grabowski, M., Meitinger, T., and Strom, T.M.; ADHR Consortium (2000). Autosomal dominant hypophosphataemic rickets is associated with mutations in FGF23. Nat. Genet. *26*, 345–348.

White, K.E., Carn, G., Lorenz-Depiereux, B., Benet-Pages, A., Strom, T.M., and Econs, M.J. (2001). Autosomal-dominant hypophosphatemic rickets (ADHR) mutations stabilize FGF-23. Kidney Int. *60*, 2079–2086.

Wu, X., Lemon, B., Li, X., Gupte, J., Weiszmann, J., Stevens, J., Hawkins, N., Shen, W., Lindberg, R., Chen, J.L., et al. (2008). C-terminal tail of FGF19 determines its specificity toward Klotho co-receptors. J. Biol. Chem. *283*, 33304–33309.

Wu, X., Weiszmann, J., Ge, H., Baribault, H., Stevens, J., Hawkins, N., Vonderfecht, S., Gardner, J., Gupte, J., Sheng, J., et al. (2012). A unique FGF23 with the ability to activate FGFR signaling through both αKlotho and βKlotho. J. Mol. Biol. *418*, 82–89.

Yamashita, T., Konishi, M., Miyake, A., Inui, K., and Itoh, N. (2002). Fibroblast growth factor (FGF)-23 inhibits renal phosphate reabsorption by activation of the mitogen-activated protein kinase pathway. J. Biol. Chem. *277*, 28265–28270.

Yie, J., Hecht, R., Patel, J., Stevens, J., Wang, W., Hawkins, N., Steavenson, S., Smith, S., Winters, D., Fisher, S., et al. (2009). FGF21 N- and C-termini play different roles in receptor interaction and activation. FEBS Lett. *583*, 19–24.

Yie, J., Wang, W., Deng, L., Tam, L.T., Stevens, J., Chen, M.M., Li, Y., Xu, J., Lindberg, R., Hecht, R., et al. (2012). Understanding the physical interactions in the FGF21/FGFR/β-Klotho complex: structural requirements and implications in FGF21 signaling. Chem. Biol. Drug Des. *79*, 398–410.

STAR★METHODS

KEY RESOURCES TABLE

REAGENT or RESOURCE	SOURCE	IDENTIFIER
Bacterial and virus strains		
E.coli: Stellar competent cells	Clontech	Cat# 636763
E.coli: OrigamiB(DE3) Novagen	Millipore Sigma	Cat# 70837-3
Chemicals, peptides, and recombinant proteins		
H-Rink-Amide-ChemMatrix resin	PCAS BioMatrix Inc	N/A
Fmoc amino acids	Midwest Biotech	N/A
Antibiotic-Antimycotic	GIBCO	Cat# 15240062
Trizol	Invitrogen	Cat# 15596018
Critical commercial assays		
AlphaLISA SureFire Ultra p-ERK1/2 (Thr202/Tyr204)	Perkin Elmer	Cat# ALSU-PERK-A10K
In-Fusion HD EcoDry Cloning Plus kit	Clontech	Cat# 638913
QIAprep Spin Miniprep Kit	QIAGEN	Cat# 27104
TaqMan RNA-to-CT One-Step kit	Applied Biosystems	Cat# 4392653
Protein Thermal Shift	Applied Biosystems	Cat# 4461146
Experimental models: cell lines		
293T HEK/hKL	Agrawal et al., 2018	N/A
293T HEK/hKLB	Agrawal et al., 2018	N/A
Experimental models: organisms/strains		
C57BL/6 female mice	Jackson labs	N/A
Oligonucleotides		
Mouse Cyp24a1	Applied Biosystems	Mm00487244_m1
Mouse Cyp27b1	Applied Biosystems	Mm01165918_g1
Mouse Egr1	Applied Biosystems	Mm00656724_m1
Mouse Actb	Applied Biosystems	Mm02619580_g1
Recombinant DNA		
FGF23	Integrated DNA technologies	UniProtKB Q9GZV9
FGF21	Integrated DNA technologies	UniProtKB Q9NSA1
FGF23 C72	Integrated DNA technologies	N/A
FGF21-23 C72	Integrated DNA technologies	N/A
FGF21-23 C26	Integrated DNA technologies	N/A
Software and algorithms		
Prism 8.0	GraphPad	N/A
Other		
HiPrep 26/10 Desalting column	Cytiva	Cat# 17508701
HiPrep Q HP 16/10 column	Cytiva	Cat# 29018182
Luna C8 column	Phenomenex	Cat# 00G-4250-P0-AX

RESOURCE AVAILABILITY

Lead contact

Further information and requests for resources and reagents should be directed to and will be fulfilled by the Lead Contact, Richard D. DiMarchi (rdimarch@indiana.edu).

Materials availability

All unique/stable reagents generated in this study are available from the Lead Contact with a completed Materials Transfer Agreement.

Data and code availability

This study did not generate any unique datasets or code.

EXPERIMENTAL MODEL AND SUBJECT DETAILS

Animals

Animal studies were performed according to the Institutional Animal Care and Use Committee (IACUC) of the Indiana University School of Medicine, which complied with the NIH guidelines. 8-9 weeks old female C57BL/6 mice were purchased from Jackson Laboratory and acclimated for one week before study. Normal rodent diet (2018SX, Harlan Teklad) and water were provided *ad libitum*.

Cell lines

293T HEK (human embryonic kidney) cells expressing human KL or human KLB (described in Agrawal et al., 2018) were cultured in DMEM High glucose GlutaMAX (GIBCO) media supplemented with 10% Fetal Bovine Serum (GIBCO) and 1x Antibiotic-Antimycotic (GIBCO) at 37 C, 95% humidity and 5% CO2.

METHOD DETAILS

Peptide synthesis

FGF23 or FGF21 peptides were chemically synthesized as C-terminal amides by Fmoc solid-phase methodology with ABI or CS336X (CSBio) automated peptide synthesizers using H-Rink-Amide-ChemMatrix resin (PCAS BioMatrix Inc) with DIC/6-Cl⁻HOBt (N,N'-Diisopropylcarbodiimide (Sigma Aldrich), 1-Hydroxy-6-chloro-benzotriazole (Aapptec) activation chemistry as described in Agrawal et al. (2018). All amino acid residues were purchased from Midwest Biotech. Peptide cleavage from the resin and side chain protection removal was done by treatment with trifluoroacetic acid (TFA) containing 2.5% triisopropylsilane, 2.5% H2O, 1% methyl sulfide and 1% 2, 2′-(ethylenedioxy)diethanethiol as scavengers for two hours. Cold ethyl ether was used for peptide precipitation, and subsequently the peptides were solubilized in 20% aqueous acetonitrile (ACN). Peptides were purified by preparative reverse phase chromatography with Waters HPLC system using a Luna C8 column (Luna 10 μm C8(2), 100 Å, AXIA-Packed LC Column 250 × 21.2 mm; Phenomenex), and a linear gradient of increasing ACN in aqueous 0.1% TFA was employed over 90 minutes. The pure fractions as analyzed by LCMS were pooled and lyophilized. Subsequently, the peptides were dissolved in PBS buffer for further tests. To test the specific peptides containing a C-terminal cysteine residue as a monomer, 10 mM β-mercaptoethanol was added to the solution, and to produce the specific dimers by cysteine-oxidation, 10% DMSO was added to the solution and incubated overnight at room temperature. The desired monomer or dimeric peptide formation was verified by LCMS.

Protein synthesis

Human FGF23 (UniProtKB #Q9GZV9: amino acid sequence 25-240), Human FGF21 (UniProtKB #Q9NSA1, 29-209), FGF21-23 C72 (FGF21 29-184 fused with FGF23 180-251), FGF21-23 C26 (FGF21 29-184 fused with FGF23 180-205), or FGF23 C72 (FGF23 180-251) cDNA sequences (Integrated DNA Technologies) were individually inserted in expression vector using In-Fusion HD EcoDry Cloning Plus kit (Clontech) as described in Agrawal et al. (2018). pET21b vector was modified to contain yeast small ubiquitin-like modifier (SUMO) sequence followed by 6xHis tag and the desired protein cDNA sequence. Site specific primers were designed (Integrated DNA technologies) for the generation of desired mutation correspondingly, and mutagenesis was performed by standard PCR method. Stellar *E.coli* competent cells (Clontech) were transformed to amplify the plasmid and the positive clones were selected by LB/Ampicillin agar plates. Plasmid harvesting was done with QIA Miniprep kit (QIAGEN) and confirmed by DNA sequencing. OrigamiB (DE3) *E.coli* cells (Novagen) were transformed for protein expression with the appropriate plasmids and the cells were cultured to 0.8-0.9 OD600 at 37 C and induced by 0.2 mM isopropyl-D-thiogalactoside (IPTG) for protein expression at 20 C overnight. The cells were harvested, lysed by sonication, and the clarified supernatant was applied to Ni-NTA column (QIAGEN) for protein enrichment. Imidazole (500 mM) containing Tris buffer was used to elute the protein and subsequently digested with SUMO protease ubiquitin-like-specific protease 1 at 4°C overnight. Pure FGF-analogs were obtained by affinity chromatography with HiPrep Q-Sepharose column (Cytiva) using fast flow liquid chromatography system (Cytiva). Tris buffer with increasing concentration of NaCl at pH 8.0 was employed for the purification of FGF21-23 chimeric analogs, while the FGF23-analogs utilized sodium carbonate/bicarbonate buffer with increasing concentration of NaCl at pH 10.5. FGF23 analogs were transferred to sterile 25 mM HEPES, 150 mM NaCl, 2% glycerol, pH 7.4 buffer for *in vivo* studies.

Purity and concentration estimation of the peptides and proteins

The purity of the biosynthesized proteins and chemically synthesized peptides was assessed by LC-MS (Agilent 1260 Infinity-6120 quadrupole mass spectrometer) as described in Agrawal et al. (2018). The analogs were analyzed by a reverse-phase Kinetex C8 column (2.6 μm, 100 Å, LC Column 75 × 2.1 mm; Phenomenex) with a linear gradient of 10%–80%B at a flow rate of 1.0 ml/min

for 10 minutes, using aqueous 0.05% TFA (A) and aqueous 0.05% TFA/90% ACN (B) as elution solvents. All proteins and peptides were obtained to > 90% purity. The concentration of each protein and peptide was determined based on their UV absorbance on NanoDrop OneC spectrophotometer (Thermo Fisher Scientific) and the extinction coefficients for the respective sequences were obtained with online tools (Prot pi peptide or ExPASy ProtParam).

pERK AlphaLISA assay

293T HEK cells expressing KL or KLB were plated to 5-6 × 10^4 cells/well density in 96-well cell culture plate coated with poly-D-Lysine (Corning). The cells were serum starved for four hours in 0.1% BSA fraction V (Thermo Fisher) containing media prior to treatment with protein or protein and antagonist peptide mixture at the mentioned concentrations for 10 minutes at 37 C as described in Agrawal et al. (2018). For the antagonist assays, 0.5 nM of FGF23 (293/KL) or 10 nM FGF21 (293/KLB) protein was added to cell treatment media to stimulate the cells for determining a baseline response. Following the respective cell treatments, the cells were lysed for 10 minutes at room temperature on a shaker and the lysate was mixed with reaction mixture as per manufacturer's protocol (AlphaLISA SureFire Ultra pERK1/2 Thr202/Tyr204, Perkin Elmer). The data were recorded by Envision plate reader (Perkin Elmer).

Protein Thermal Shift

FGF23 proteins were analyzed for their thermal denaturation characteristics with the Applied Biosystems QuantStudio 3 instrument, using the protein thermal shift dye (Life Technologies) across a temperature gradient of 25 to 95°C in quadruplicates. The average of the first order derivative curve of the florescence intensity is plotted in the graph using GraphPad Prism 8 software, and was used to determine the melting temperature (Tm).

In vivo studies

After being acclimated for 1 week, the mice were treated with a single dose of 30 mg/kg body weight FGF23 antagonist peptide 6 or saline by i.p. administration (n = 5 or 6/group). The mice were euthanized after 3- or 24-hours, and the kidneys were removed at necropsy and analyzed.

For the FGF23-signaling studies, FGF23 analog was administered as a single i.p. dose of 0.5 mg/kg body weight, n = 5/group for Vehicle and FGF23 $A^{188,222}$, n = 10/group for FGF23, FGF23 A^{188}, and FGF23 A^{222}. The mice were euthanized after 3-hours and the kidneys were harvested and analyzed.

Quantitative real time PCR

Mouse kidney RNA was extracted using Trizol (Life Technologies), following the manufacturer's protocols and tested by qRT-PCR with primers specific for mouse *Cyp24a1*, *Cyp27b1, Egr1* and *Actb* in duplicates (Applied Biosystems). The TaqMan One-Step RT-PCR kit (Life Technologies) was used for all experiments, and data were collected with a 7500 Real Time PCR/StepOne Plus system and software (Life Technologies). The qPCR data were analyzed using the 2-ΔΔCT method according to Livak and Schmittgen (2001) and the graph was plotted in GraphPad Prism 8.

Structural modeling of C28 peptide

Structure of FGF23/FGFR/KL ternary receptor complex (PDB 5W21, Chen et al., 2018) was used as a template where $FGF23^{181-205}$ (C26) sequence was replaced with $FGF23^{212-239}$ (C28) to generate a model structure using SWISS-MODEL (https://swissmodel.expasy.org/). The C28 peptide model was then superimposed on the known C26 structure using PyMOL.

QUANTIFICATION AND STATISTICAL ANALYSIS

Cellular signaling data analysis

All cellular phosphorylation data were analyzed using 3-parameter non-linear regression curve in GraphPad Prism 8 as described in Agrawal et al. (2018). Graphs are plotted to represent the relative (%) activities of analogs as adjusted by the maximal (100%) response obtained from the positive control. For antagonistic assays, the difference between the pERK signal at baseline (fixed dose of FGF-stimulation, no antagonist peptide) and the highest dose of the positive control C26, C28, C72, peptide 6 or 21C25 was used to calculate the maximal response (100%) correspondingly. Similarly, for an agonist assay the difference between the pERK signal of baseline (only cell culture medium, no agonist) and the highest dose of the positive control FGF23 in 293/KL cells was used to establish the maximal (100%) response. Each peptide and protein analog were tested in triplicates in three independent experiments (n = 3), and the normalized graphs are presented with mean ± SD.

Gene expression data analysis of *in vivo* studies

Statistical analyses of the peptide antagonist study data were performed using two-tailed, unpaired t test followed by Bonferroni adjustment, and $p < 0.05$ were considered significant. Statistical analyses of the FGF23-agonist studies were performed by one-way ANOVA followed by Tukey's comparison, and $p < 0.05$ were considered significant. Means and standard errors of the mean are shown in the graphs.